T lymphocyte passive deformation is controlled by unfolding of membrane surface reservoirs

Lionel Guillou[a], Avin Babataheri[a], Michael Saitakis[b], Armelle Bohineust[b,c], Stéphanie Dogniaux[b], Claire Hivroz[b], Abdul I. Barakat[a], and Julien Husson[a1]

[a]Laboratoire d'Hydrodynamique (LadHyX), Ecole polytechnique, CNRS UMR 7646, 91128 Palaiseau, France.

[b]Institut Curie, INSERM U932, PSL Research University, F-75005, Paris, France.

[c]Institut Pasteur, INSERM U668, Dynamics of Immune Responses Unit, 75015 Paris, France.

[1]To whom correspondence should be addressed. E-mail: julien.husson@ladhyx.polytechnique.fr

RUNNING HEAD

T lymphocyte passive deformation

HIGHLIGHT SUMMARY

T lymphocyte passive deformation when squeezing through narrow capillaries is limited by the excess membrane contained in microvilli and membrane folds. During active processes, such as transendothelial migration, larger deformations are made possible by an increase in membrane area, possibly through recruitment of internal membrane reservoirs.

ABSTRACT

T lymphocytes in the human body routinely undergo large deformations, both passively when going through narrow capillaries and actively when transmigrating across endothelial cells or squeezing through tissue. We investigate physical factors that enable and limit such deformations and explore how passive and active deformations may differ. Employing micropipette aspiration to mimic squeezing through narrow capillaries, we find that T lymphocytes maintain a constant volume while increasing their apparent membrane surface area upon aspiration. Human resting T lymphocytes, T lymphoblasts and the leukemic Jurkat T cells all exhibit membrane rupture above a critical membrane area expansion that is independent of either micropipette size or aspiration pressure. The unfolded membrane matches the excess membrane contained in microvilli and membrane folds, as determined using scanning electron microscopy. In contrast, during transendothelial migration, a form of active deformation, we find that the membrane surface exceeds by a factor of two the amount of membrane stored in microvilli and folds. These results suggest that internal membrane reservoirs need to be recruited, possibly through exocytosis, for large active deformations to occur.

INTRODUCTION

The ability of T lymphocytes to both patrol the vasculature and to extravasate into surrounding tissue is a central feature of the human adaptive immune response (von Andrian and Mempel, 2003; Valignat *et al.*, 2013; Crotty, 2015; DuPage and Bluestone, 2016). Accomplishing these tasks requires T lymphocytes to undergo large deformations, both passively as they move through narrow capillaries during their patrols (Fung, 2013), and actively upon extravasation at a site of inflammation or injury (Carman and Springer, 2004; Carman, 2009; Carman and Martinelli, 2015). In certain cell types, for instance neural cells during brain trauma, excessive strain can cause membrane damage both *in vitro* (Geddes *et al.*, 2003) and *in vivo* (Pettus *et al.*, 1994; Pettus and Povlishock, 1996). To our knowledge, however, there have been no reports of T lymphocyte membrane damage *in vivo* despite the large deformations that these cells undergo. In the present study, we wanted to understand how T lymphocytes respond to large passive deformations. We asked specifically if there was a physical criterion for these deformations to trigger membrane rupture and whether or not this criterion changed during the life of a T lymphocyte (when the resting T lymphocyte becomes a lymphoblast). Finally, we investigated whether such a criterion would also apply to large active deformations as occurs during cell spreading and extravasation.

RESULTS

A T lymphocyte increases its surface area at constant volume when entering in a narrow capillary

To mimic the partial or complete passage of T lymphocytes through a narrow capillary *in vivo*, we aspirate T lymphocytes into glass micropipettes of a few microns in diameter. Indeed, the relevant length scale here is the micron, given that human capillary diameters are in the range of 5-10 µm (Fung, 2013) and that, based on our own measurements, resting T lymphocytes have a diameter of 6.7 ± 0.4 µm (mean ± SD). Active migrations of T lymphocytes also occur at the same length scale, as previous studies have measured pore sizes from transendothelial migration of T lymphocytes to be close to 5 µm (Carman and Springer, 2004; Shulman *et al.*, 2011).

After grabbing T lymphocytes using a small aspiration pressure (10 to 20 Pa), we apply a constant aspiration pressure ΔP (Figure 1A) and observe the entry of the aspirated cell for 5 minutes. Measuring the cell dimensions before and after this aspiration period, we show that cell volume is constant regardless of the T lymphocyte activation state, the aspiration pressure or the capillary size (Figure 1B and Supplementary Figure S1). We note that the volumes seen here for T lymphocytes are consistent with what we find using fluorescent staining and confocal microscopy (Supplementary Figure S2). The preservation of the volume during aspiration is consistent with the fact that applied aspiration pressures, on the order of ~10-1000 Pa, are much lower than the cellular osmotic pressure of ~10^6 Pa acting to maintain the cell volume constant. The value for osmotic pressure was derived using the van't Hoff law, assuming a cell osmolality of ~300 mOsm for white blood cells, as measured by Schmid-Schönbein *et al.* (Schmid-Schönbein *et al.*, 1980). In order to accommodate the constant volume constraint during aspiration, cells depart from their initial relatively spherical shape, which is the geometric shape that minimizes surface area for a given volume. As a result, their surface area increases, so that the membrane of a T lymphocyte is stretched when it passes through a capillary.

Surface area expansion of T lymphocytes is accompanied by an increase in cell stiffness

In order to determine if resting T lymphocytes respond mechanically to passive deformations undergone during their aspiration into a micropipette, we measure the evolution of their effective stiffness as determined by microindentation. Microindentation consists of applying a known compressive force to a T lymphocyte while measuring the resulting indentation (Figure 2 and Supplementary Movie 1). Using a model linking the applied force to the measured deformation allows the

extraction of the mechanical parameters of the cell, such as its elastic properties (Guillou *et al.*, 2016).

First, we find that resting T lymphocyte behavior upon indentation is consistent with an elastic solid model. Indeed, the force-indentation curves we obtain are well described by the classical Hertz model, which is a standard model used to describe the indentation of an elastic solid (Johnson, 1985) often employed to analyze atomic force microscopy experiments (Dimitriadis *et al.*, 2002; Krause *et al.*, 2013). In this model, the indentation force, F, applied to an incompressible elastic substrate is related to the resulting indentation of this medium, δ, through the relationship $F = 16/9\ E\ \delta^{3/2}$. Thus, the force is directly proportional to the Young's modulus of the material E, which measures the elasticity of the medium (expressed in Pascals), and to the indentation raised to the power 3/2. As other types of elastic behavior exist, which are described by an exponent of the indentation other than 3/2 (Lomakina *et al.*, 2004), we fit our data using a more general relationship $F = \alpha\ \delta^{\beta}$, where α and β are adjustable fitting parameters. We find that $\beta = 1.55 \pm 0.14$ (mean ± SD) for a set of 201 cell indentations (Figure 2C), in excellent agreement with the prediction of the Hertz model of $\beta = 3/2$ (see example curve in Supplementary Figure S3). From the fitted value of $\alpha = 16/9\ E$ we deduce that E = 77 ± 8 Pa (mean ± standard error of the mean) when the cell membrane is not stretched.

Second, we find that the effective cell stiffness increases with the apparent membrane surface area (Figure 2D). The increase in apparent membrane surface area is evaluated by tracking the ratio A/A0, where A is the apparent membrane surface area at the time of indentation, and A0 is the initial apparent membrane surface area. To test if this increase in cell stiffness depends on the applied aspiration pressure, we submit cells to a constant pressure while monitoring both the effective stiffness and the ratio A/A0. We find that both increase continuously under a constant aspiration pressure (Figure 2E). When different aspiration pressures are applied, the relationship between the effective stiffness and the apparent membrane surface area remains the same, i.e. the data points lie on the same E = f(A/A0) curve. Furthermore, the relationship is reversible, in the sense that when aspiration pressure is reset to a low level (typically 10-20 Pa), both effective stiffness and apparent membrane surface decrease, following the same conserved relationship (see Figure 2E and Supplementary Figure S4 for details). Interestingly, we note that this reversibility appears to depend on the activity of myosin-II. Indeed, disrupting myosin-II activity with blebbistatin prevents the apparent stiffness from returning to its baseline value (Supplementary Figure S5). This shows that, consistent with previous work (Spinler *et al.*, 2015), myosin-II activity influences the cell behavior in reaction to micropipette aspiration. In any case, we find that – similar to the approaches of Herant *et al.* and Lam *et al.* (Herant *et al.*, 2005; Lam *et al.*, 2009) – the relationship E = f(A/A0) is well described by the following phenomenological law:

$$\begin{cases} E = E0 \text{ for } A/A0 < (1+\varepsilon) \\ E = E0 + k\,(A/A0 - (1+\varepsilon)) \text{ for } A/A0 > (1+\varepsilon) \end{cases}$$

(fit in Figure 2D), where E0 is the initial effective stiffness, k is an elastic expansion modulus and ε is a measure of membrane slack, corresponding to the fraction of initial apparent membrane surface area that can be taken before it is necessary to unfurl folds or microvilli. Fitting our data with this relation, we find E0 = 77 ± 8 Pa (mean ± standard error of the mean) (see Supplementary Table T1 for details on the other two fitting parameters). This finding is consistent with a previous estimate of human primary CD4+ T lymphocytes' stiffness of 85 ± 5 Pa using a parallel plates technique (Bufi *et al.*, 2015). We note that the same study measured a very similar stiffness of 90 ± 10 Pa for Jurkat cells, which means that any difference in behavior that may be seen during micropipette aspiration between the two cell types is not attributable to differences in cell stiffness.

Previous micropipette aspiration experiments have shown that membrane expansion is directly associated with an increase in cell tension γ for both neutrophils (Herant *et al.*, 2005) and macrophages (Lam *et al.*, 2009). In fact, the dependence of cell tension on membrane expansion takes the same form as we found for effective stiffness:

$$\begin{cases} \gamma = \gamma 0 \text{ for } A/A0 < (1+\varepsilon) \\ \gamma = \gamma 0 + k\,(A/A0 - (1+\varepsilon)) \text{ for } A/A0 > (1+\varepsilon) \end{cases}$$

(Lam *et al.*, 2009). Hence, the increase in effective stiffness we measure here is a direct indication that cell tension also increases. The connection between these two mechanical properties is further supported by recent experiments that show that the effective stiffness of a non-adherent cell, as measured by microindentation, is directly related to its cortical tension via the relation $E = \gamma^2 (\pi D0)/(4hF)$ (Cartagena-Rivera *et al.*, 2016). In this relation, E is the apparent stiffness of the cell, γ its cortical tension, D0 the cell diameter, h the cell's cortical thickness, and F the indentation force. Taken together, these results show that apparent membrane surface area is a good predictor of cell mechanical properties.

T lymphocyte membrane ruptures at a well-defined entry length for a given capillary size

Beyond measuring how effective stiffness is reversibly linked to an increase of cell apparent area, we seek to understand if it is possible to induce permanent damage to a T lymphocyte by forcing it through a narrow capillary. To do so, we again employ micropipette aspiration as a proxy for passage into capillaries and use propidium iodide as a reporter of membrane rupture (Figure 3 A-C and Supplementary Movies 2-4).

We observe that the membrane of resting T lymphocytes ruptures at a well-defined entry length $L^* = 6.3 \pm 1.1$ µm (mean ± SD) for micropipette diameters Dp varying between 2.0 and 2.8 µm (Figure 3D). For larger micropipette diameters, the membrane of resting T lymphocytes does not rupture, as cells are entirely aspirated into the pipette, provided that a sufficient aspiration pressure is applied. Because of the experimental difficulties associated with performing micropipette aspiration with micropipettes below 2.0 µm in diameter, the range of micropipette diameters explored for resting T lymphocytes is *de facto* limited to values between 2.0 and 3.0 µm. As mentioned previously, physiological pore sizes are typically slightly larger than that, with capillary diameters usually larger than 5 µm (Fung, 2013) and pore sizes from transendothelial migration close to 5 µm (Carman and Springer, 2004; Shulman *et al.*, 2011). The implications of that observation are examined in the discussion section.

To further explore the effect of micropipette diameter on membrane rupture, we perform micropipette aspirations on Jurkat cells, a leukemic T cell line commonly used as a model for T lymphocytes. Jurkat cells are larger than resting T lymphocytes, with an average diameter $D0 = 10.6 \pm 1.0$ µm (mean ± SD) compared to $D0 = 6.7 \pm 0.4$ µm (mean ± SD) for resting T lymphocytes, and therefore allow a wider range of micropipette diameters. We find that while the entry length at rupture L^* is still a well-defined quantity for a given micropipette diameter Dp, L^* decreases as Dp increases (Figure 3D). Also, we note that for a given micropipette diameter, the entry length at rupture is much greater for Jurkat cells than for resting T lymphocytes.

Activated T lymphocytes, also referred to as lymphoblasts, are much more effective at extravasating than resting T lymphocytes (Springer, 1994). This is due to the increased expression of receptors to certain chemokines and adhesion molecules. Yet mechanical and morphological properties of these activated T lymphocytes might also contribute to these functions. Thus, to understand how activating T lymphocytes affects their ability to deform, we perform micropipette aspirations on lymphoblasts. We find that lymphoblasts are slightly larger than resting T lymphocytes with an initial diameter D0 of 8.1 ± 0.7 µm (mean ± SD) and that their entry length at rupture $L^* = 19.0 \pm 9.2$ µm (mean ± SD) is 3 times as large as that of resting T lymphocytes (Figure 3D). Activation therefore considerably increases a T lymphocyte's ability to deform its membrane.

Maximum deformation of T lymphocyte at rupture does not depend on aspiration pressure

In order to test if the value of aspiration pressure affects the maximal entry length at rupture, L^*, we vary aspiration pressure while holding the micropipette diameter constant. We find that, for a given micropipette diameter Dp, L^* does not depend on the aspiration pressure for both resting T lymphocytes and Jurkat cells (Figure 4A).

This shows that neither the level of aspiration pressure nor the duration of aspiration are intrinsic parameters to describe membrane rupture of T lymphocytes. Nonetheless, higher aspiration pressures lead to shorter rupture times, as the cell entry into the micropipette occurs faster (Figure 4B). Consistent with this notion, a previous study by Hategan *et al.* also found that higher aspiration led to faster lysis of red blood cells (Hategan *et al.*, 2003). Strain rates in those experiments were comparable to albeit somewhat smaller than ours. Indeed, for T lymphocytes, our strain rates were on the order of ~1-10 $\mu m^2/s$, whereas Hategan *et al.* reported strain rates for red blood cells on the order of ~0.1-1 $\mu m^2/s$.

Moreover, we find that cell rupture can be located anywhere along the cell circumference, i.e. either in the distal or proximal portions of the cell, with no particular preference. Therefore, any mechanism of cell rupture that tends to favor a rupture location, such as the nucleus acting as a piston which would create a pressure accumulation in the distal part of the cell as discussed by Petrie *et al.* (Petrie *et al.*, 2014), seems unlikely with respect to our experimental observations.

T lymphocyte membrane rupture occurs at a critical apparent membrane expansion

To elucidate the factor limiting passive deformations of T lymphocytes, we seek to obtain a criterion that is predictive of T lymphocyte membrane rupture. As noted above, cell volume is conserved during micropipette aspiration, so that the apparent membrane surface area increases as soon as the cell departs from a spherical shape that minimizes its surface area. Membrane expansion is again defined as the ratio between the apparent membrane surface area A divided by the initial apparent membrane surface area A0. Computing this membrane expansion across all the capillary sizes tested, we find that a critical membrane expansion defining a threshold beyond which membrane rupture is a criterion that predicts our data for both resting T lymphocytes and Jurkat cells fairly accurately (Figure 5). We find a critical membrane expansion $A^*/A0 = 1.22 \pm 0.09$ and $A^*/A0 = 1.48 \pm 0.15$ (mean ± SD) for resting T lymphocytes and Jurkat cells, respectively, where A* is the apparent membrane surface area at rupture. Lymphoblasts, on the other hand, show more variability, with $A^*/A0 = 1.36 \pm 0.27$ (mean ± SD). In the case of Jurkat cells, we also observe that for larger micropipette diameters, the critical membrane expansion decreases slightly, a possible bias being that large micropipette diameters are associated with lower aspiration pressures and shorter rupture times (Supplementary Figure S6). It is therefore possible that, in Jurkat cells, membrane expansion is favored by a longer squeezing time.

Moreover, we investigate how the state of the cytoskeleton might affect this membrane expansion at rupture. To do so, we incubate the cells in 1 µM latrunculin B for at least 60 min to disrupt cortical actin polymerization (Wakatsuki *et al.*, 2001).

We find that the membrane expansion at rupture A*/A0 for resting T lymphocytes increases from 1.22 ± 0.09 (mean ± SD, n = 14 cells) in the control case to 1.41 ± 0.15 (n = 9 cells) for cells treated with latrunculin B and from 1.36 ± 0.27 (n = 14 cells) to 1.42 ± 0.16 (n = 23 cells) for lymphoblasts. Hence, in both cases, depolymerizing actin increases the membrane expansion at rupture, up to a maximum value of ~40%.

While our rupture criterion relates to membrane expansion, it is still consistent with a criterion based on a threshold in cell tension as used by others to describe the rupture of the membrane of fibroblasts (Tan *et al.*, 2011) or lipid vesicles (Evans *et al.*, 2003). In fact, as mentioned before, previous investigators have found that cell tension and membrane expansion are directly related in neutrophils (Herant *et al.*, 2005) and macrophages (Lam *et al.*, 2009). In our experiments, Laplace's law, while imprecise outside equilibrium, allows us to roughly estimate the cell tension at rupture γ^*. We find that $\gamma^* = 0.5 \pm 0.4$ mN/m (mean ± SD) for resting T lymphocytes, 1.2 ± 0.9 mN/m for lymphoblasts and 1.3 ± 0.8 mN/m for Jurkat cells. Interestingly, these values are close for all cell types, suggesting that this critical tension is an intrinsic mechanical parameter shared by different cell types. However, this critical value might be different for adherent cells, as Tan *et al.* who used micropipette aspiration to rupture the membranes of fibroblasts, found a higher – although consistent – value of γ^*~3 mN/m at rupture (Tan *et al.*, 2011).

The amount of membrane deployed by T lymphocytes before rupture matches the stock of membrane contained in microvilli and membrane folds

While T lymphocytes may appear smooth (with some ruffles in the case of lymphoblasts and Jurkat cells) under optical microscopy, observations at the submicron scale under scanning electron microscopy reveals that the surface of T lymphocytes is covered with microvilli and membrane folds (Figure 6). For resting T lymphocytes and lymphoblasts, we mainly see microvilli, while for Jurkat cells, most of the excess membrane is found in the form of membrane folds.

The excess membrane contained in the microvilli of resting T lymphocytes has been previously estimated using scanning electron microscopy (Majstoravich *et al.*, 2004). To do so, Majstoravich *et al.* assumed a cylindrical shape for microvilli and measured the microvilli density (4.1 per μm^2), average length (380 nm) and average diameter (100 nm). This led them to estimate a relative excess membrane of ~49% for resting T lymphocytes. We note that earlier work in the 1980s that used a combination of transmission electron microscopy and stereology found values ranging from 21% (Boesen and Hokland, 1982) to ~130% (Schmid-Schönbein *et al.*, 1980).

We follow the same approach as Majstoravich *et al.* using scanning electron microscopy. We preferred this method to alternatives, i.e. transmission electron microscopy combined with stereology (Schmid-Schönbein *et al.*, 1980; Boesen and

Hokland, 1982) and a capacitance-based method (Ross *et al.*, 1994) for two reasons: 1) it is a direct and hence essentially model-independent measurement, and 2) it appears to lead to less variable results. For lymphoblasts, we find a microvilli density of 6.9 per μm^2, a length of 284 ± 140 nm (mean ± SD) and a diameter of 62 ± 13 nm (mean ± SD) (Figure 6D,E). This translates to a relative excess membrane of ~40% for lymphoblasts.

For Jurkat cells, we take a slightly different approach. Indeed, we do not see as many microvilli on the surface of Jurkat cells, but we see many more membrane folds (Figure 6 A,C). Therefore, instead of assuming that the excess membrane is contained in cylindrical microvilli, we assume that most of the excess membrane is in the form of infinitesimally fine membrane folds whose height can be estimated for a given cell using the folds seen in profile. Using this approach, we find a relative excess membrane of ~41% for Jurkat cells. Consistently with this estimate, an earlier study that used capacitance, as measured by patch clamping, as an indirect method to estimate surface area, found that Jurkat cell had an external membrane reservoir of ~40-70% of their apparent membrane surface area (Ross *et al.*, 1994).

To assess if the membrane stored in ruffles and microvilli is sufficient to explain the deformation of T lymphocytes in micropipettes, we compare the maximum membrane surface area deployed using micropipette aspiration (defined as the apparent membrane surface area at rupture A* minus the initial apparent membrane surface area A0) with the excess membrane surface area contained in microvilli and folds and find that they are in good qualitative agreement for resting T lymphocytes, lymphoblasts and Jurkat cells (Figure 6F). Consistently with this picture, others showed that, upon osmotic swelling, Jurkat cell membrane ruptures if the surface area increases beyond what is contained in their external membrane reservoir (Ross *et al.*, 1994).

T lymphocyte membrane expansion during active deformation can greatly exceed the limit observed in passive deformation

In order to determine how our criterion of maximum membrane expansion for passive deformations applies to active deformations, we reproduce *in vitro* two situations in which the T lymphocyte is activated: one in which a T lymphoblast migrates across an endothelial monolayer (Figure 7 and Supplementary Movie 5), and one in which it spreads on an activating surface (Figure 7). Both were chosen because we expect the apparent membrane surface area to increase substantially and because they occur on time scales comparable to the micropipette aspiration experiments (~3 min for transendothelial migration and ~20 min for cell spreading).

We find that in both cases, the apparent membrane surface area reaches values that are much larger than the limit found in passive deformations, with an area of 526 ±

98 μm^2 (mean ± SD) after transendothelial migration and 489 ± 103 μm^2 (mean ± SD) after cell spreading. These values are similar to each other and both statistically significantly higher than the initial apparent membrane surface area of lymphoblasts, 213 ± 26 μm^2 (mean ± SD), and their apparent membrane surface area at rupture upon micropipette aspiration, 288 ± 64 μm^2 (mean ± SD).

DISCUSSION

The amount of membrane surface reservoirs is predictive of T lymphocyte membrane rupture

We showed that the amount of membrane area expansion is predictive of membrane rupture of T lymphocytes passing through narrow capillaries and that the limiting factor is the amount of excess membrane contained in microvilli and membrane folds. This result holds regardless of whether the T lymphocyte is activated or not (resting T lymphocyte and T lymphoblast) and regardless of whether it is a primary cell or a leukemic cell (primary T lymphocytes and Jurkat T cell). We therefore speculate that there could be a degree of generality to these results and that they may also be valid for other types of leukocytes. This is supported by the observation made by Evans *et al.* that the excess membrane area of granulocytes is what enables them to pass through capillaries as small as 2.6 µm in diameter (Evans and Kukan, 1984).

Membrane surface reservoirs allow T lymphocytes to pass unharmed through the microvasculature

We have shown that T lymphocytes, when aspirated into a micropipette, retain a constant volume and that beyond a critical membrane expansion of ~20% to ~50% (depending on the cell type), T lymphocyte membrane ruptures. T lymphocytes passing through a capillary assume a sausage-like shape (a cylinder with two hemi-spherical caps, see Supplementary Movie 6), similar to what has been reported for chondrocytes and neutrophils (Hochmuth, 2000). Given that their volume is also known (as it remains unchanged), we are able to compute mathematically the apparent membrane surface area A of a T lymphocyte passing through a capillary of a given size (following the method detailed in Supplementary Figure S1). Because we also have access to the initial apparent membrane surface area A0 (by measuring the initial T lymphocyte diameter), we can compute the membrane expansion A/A0 associated with a given capillary size (this is shown, for a T lymphocyte of average size, by the line separating the green zone from the red and black zones in Figures 5A-C). We see that the smaller the capillary, the higher the T lymphocyte membrane expansion needs to be to pass through it. Further, because we have shown previously that T lymphocytes rupture at a critical membrane expansion (shown by the line separating the red and black zone in Figures 5A-C), this means that for each type of T

lymphocyte, there exists a critical capillary size under which the T lymphocyte will either be trapped or rupture depending on the pressure exerted on it. This critical diameter is given by the intersection of the two lines in the "phase diagrams" (by analogy with physical phase diagrams) on Figures 5A-C. We deduce a minimum capillary size of 4.1 µm for resting T lymphocytes, 4.2 µm for lymphoblasts and 5.1 µm for Jurkat cells.

Human capillaries are in the range of 5-10 µm (Fung, 2013), which is in some cases smaller than the typical size of a T lymphocyte but always sufficiently large for the T lymphocyte to pass through without risking membrane rupture or getting trapped, according to our results. Therefore, we suggest that the excess membrane contained in the microvilli and membrane folds of T lymphocytes is tightly regulated to enable them to pass unharmed through the microcirculation.

Pore size during extravasation is determined by T lymphocyte, not endothelial cell

Our *in vitro* transmigration assay allows for the quantification of the endothelial pore size during T lymphocyte transmigration. We find a diameter of 5.1 ± 0.5 µm. Consistent with this value, images from previous studies indicate pore sizes from transmigrating T lymphocytes of 5.3 µm (Carman and Springer, 2004) and 5.4 µm (Shulman *et al.*, 2011). Importantly, we observe that the pore size increases with cell size (Figure 7B), which suggests leukocytes and not endothelial cells determine the size of this pore. Furthermore, the pore size is comparable to the size of the smallest capillaries that a T lymphocyte may find itself going through without rupture. Hence, the pore size might be an optimum that minimizes the mechanical effort needed to create it, while also minimizing the risk of leukocyte membrane damage during transmigration.

Active deformations of T lymphocytes require more membrane than is available in surface reservoirs

We have shown that the membrane surface area of lymphoblasts during cell spreading and transendothelial migration is ~200-250 µm^2 higher than the external membrane surface area of lymphoblasts, even when accounting for microvilli and membrane folds. This means that additional membrane must be recruited during active deformations. We propose that this is enabled by internal membrane reservoirs, possibly through exocytosis.

Indeed, there are numerous examples where cells have been shown to recruit additional membrane through exocytosis to enable large active deformations. For cell spreading, there is direct evidence in fibroblasts that the increase in membrane surface area is enabled by exocytosis (Gauthier *et al.*, 2011). Similarly, during

phagocytosis, the dramatic increase in macrophage membrane surface area is enabled by exocytosis (Hackam *et al.*, 1998; Bajno *et al.*, 2000; Niedergang *et al.*, 2003; Braun *et al.*, 2004). Drosophila cellularization provides yet another example. Indeed, exocytosis has been shown to add membrane to the cell surface to enable the furrow ingression needed for cellularization (Figard *et al.*, 2013). Finally, multiple cell types (AS49, 16HBE 140-, CHO and NIH 3T3 cells) have been observed to use exocytosis to enable expanding volumes during hyposmotic swelling (Groulx *et al.*, 2006). Interestingly, Groulx *et al.* remarked that the membrane surface area can increase 3.6 fold under normal conditions but only 1.7 fold when exocytosis is blocked. This difference in membrane surface area is consistent with the difference we observed between passive and active deformations. Indeed, during passive deformations, we saw a 1.2-1.5 fold increase in membrane surface area, whereas during active deformations, we saw a ~2.5 fold increase in membrane surface area for lymphoblasts. The difference between the two cases would presumably be made up by exocytosis, as in hyposmotic swelling. Hence, we speculate that numerous active cell processes involving large deformations, including cell spreading and transendothelial migration, but also phagocytosis and even embryonic development for some species, could be dependent on exocytosis.

MATERIALS AND METHODS

Cell purification and culture

All cells used in this study were human cells. This study was conducted according to the Helsinki Declaration, with informed consent obtained from the blood donors, as requested by the Etablissement Francais du Sang.

Human primary CD4+ T lymphocytes were negatively selected from PBMCs isolated from blood of healthy donors with the CD4 T cell isolation kit (#130-096-533, Miltenyi Biotec) as described previously (Chemin *et al.*, 2012).

To obtain CD4+ T lymphoblasts, 6-well plastic plates were coated with anti-CD3 (OKT3 clone, # 16-0037-85 from eBioscience 2.5 μg/ml in 1.3 ml final) overnight at 4°C. Wells were washed and $5.4x10^6$ purified primary human CD4+ T cells were plated per well in the presence of soluble anti-CD28 (LEAF Purified anti-human CD28 # BLE302923 – Biolegend ,2.5 μg/ml) and recombinant IL-2 (20 U/ml). Fresh medium containing IL-2 (20 U/ml) was added every 3 days and lymphoblasts were used from day 6.

Jurkat cells (clone 20; obtained from Dr. A. Alcover, Pasteur Institute, Paris, France) were grown in Glutamax-containing RPMI 1640 (Invitrogen Life Technologies, Carlsbad, CA) supplemented with 10% fœtal calf serum as described previously (Blanchard *et al.*, 2002).

Primary human aortic endothelial cells (HAEC) were purchased from ThermoFisher Scientific and cultured in medium 200 (M200500, ThermoFisher Scientific) supplemented with low serum growth supplement (S00310, ThermoFisher Scientific). They were passaged three times a week using trypsin followed by resuspension in fresh medium.

Optical microscopy

In all micropipette aspiration, profile microindentation and transendothelial migration experiments, the petri dish containing cells was mounted on a TE300 inverted microscope (Nikon Instruments, Tokyo, Japan) placed on an air suspension table (CVI Melles Griot, Netherlands). The microscope was equipped with a 100x oil immersion, 1.3 NA objective (Nikon Instruments) for experiment monitoring and lower magnification objectives (40x, 20x, 10x, and 4x, Nikon) for micropipette positioning. Images were acquired using a Flash 4.0 CMOS camera (Hamamatsu Photonics, Hamamatsu City, Japan).

Micropipette aspiration

Micropipette aspiration experiments were performed using a micropipette connected to a water reservoir, as described previously (Guillou *et al.*, 2016). We left the micropipettes in complete medium for at least 5 minutes before starting experiments to avoid cell adhesion to the micropipette wall. Propidium iodide (Sigma-Aldrich) at a concentration of 40 µg/mL was used as a reporter of membrane rupture. For membrane rupture experiments, we left a background of brightfield light to visualize the cell before rupture. The fluorescent signal from the propidium iodide was sufficiently intense to be visible despite this light. Image sequences were acquired using Micro-Manager (Vale Lab, UCSF) (Edelstein *et al.*, 2010).

Profile microindentation

To perform microindentations, cells were held using a micropipette and indented using a thin glass capillary, as described previously (Guillou *et al.*, 2016). Briefly, we impose a displacement to the base of the glass capillary using a piezoelectric controller (TPZ001, Thorlabs), and monitor the position of the capillary tip by using optical microscopy combined with cross-correlation image analysis. We used a microindenter of stiffness 0.54 nN/µm and radius 11 µm whose base we displaced at a speed of 0.5 µm/s. For the profile microindentation experiments with blebbistatin, the cells were incubated for one hour before the experiment in 50 µM blebbistatin

(B0560-1MG, Sigma). Blebbistatin at the same concentration was then left in the medium for the duration of the microindentation experiments.

Transendothelial migration

For transendothelial migration experiments, HAEC were grown to confluence in thin-bottom Petri dishes (FluoroDish 35 mm, World Precision Instruments), and inflamed overnight in TNF-α (CYT-252-5µg, Biovalley) at a concentration of 50 ng/mL. The next morning, the TNF-α was washed twice with HAEC medium. The Petri dish was then placed in a custom-made Plexiglas chamber to maintain the temperature at 37 °C. The chamber was heated by heating pads (Radiospare) connected to an electrical generator (ALR3002M, ELC) via a PID controller. The target temperature of the PID was set to 40 °C, with the input temperature to the PID given by a thermocouple placed inside the chamber at a fixed location. The chamber was also sealed at the top to minimize air flow and temperature gradients. Further, the objective was heated at a target temperature of 40 °C using an objective heater (Okolab). Both target temperatures were chosen after control experiments revealed that the actual temperature of the medium inside the Petri dish was 37 °C (as measured by a thermocouple inside the medium) when the target temperatures were both set to 40 °C. After waiting 20 min for the temperature to equilibrate inside the HAEC medium, 500 mL of lymphoblasts at a concentration of ~10^6 cells/mL were injected using a 1 mL pipette. Brightfield images were then acquired every 15 seconds for a period of 60 min, under 10x magnification.

Data analysis

Images were analyzed using ImageJ (US NIH), and data were analyzed using a custom written Matlab (Mathworks) code. Data are reported as mean ± standard deviation, both in the text and in plots, unless specified otherwise. Samples were deemed statistically significantly different (*) for $p < 0.05$ using Student's unpaired t-test. (***) indicates $p < 0.001$.

Scanning electron microscopy

Scanning electron microscopy was performed on T lymphocytes ($1.50x10^5$) incubated for 20 min at room temperature on slides pre-coated with 0.02% poly-L-lysine alone (or followed by incubation with anti-CD3 (OKT3 clone, # 16-0037-85 from eBioscience) and anti-CD28 (LEAF Purified anti-human CD28 # BLE302923 – Biolegend) at 10µg/ml, overnight at 4°C). The cells were then washed in phosphate buffer pH 7.4 (PB), fixed overnight at 4°C in PB + 2% glutaraldehyde, and finally

washed in PB. Samples were then dehydrated by passing through a graded series of ethanol solutions, then dried by the CO_2 critical-point method (CPD75 Quorum Technologies) and coated by sputtering with a 20-40 nm gold thin layer using a Scancoat Six (Edwards). Acquisitions were performed using a GeminiSEM 500 (Zeiss), except for the cell spreading experiments for which acquisitions were performed using a Cambridge Stereoscan 260.

Fluorescent staining and confocal microscopy for cell volume measurement

Cells were fluorescently stained and their volume measured using a confocal microscope as detailed previously (Bufi *et al.*, 2015). Briefly, cells were plated on fibronectin (10 µg/mL, Sigma-Aldrich)-coated glass coverslips, fixed, permeabilized and stained for DAPI (Life Technologies) and phalloidin-Alexa-546 (Life Technologies). The samples were observed on an inverted spinning-disk confocal microscope Nikon TiE (Nikon, Tokyo, Japan) equipped with a piezo-stage NanoScanZ mounted on a Marzhauser XYZ motorized scanning stage. Three-dimensional stacks of images were acquired with a step of 0.2 mm using a 100x immersion oil objective and an EM-CCD iXon 897 Andor camera (Andor, Belfast, UK). Images were analyzed using the ImageJ software.

ACKNOWLEDGEMENTS

The authors acknowledge Caroline Frot, Antoine Garcia, Daniel Guy, Delphine L'Huillier, Magali Tutou, and Do Chi Toai Vu at LadHyX for technical support. The authors also acknowledge Virginie Bazin from the Electron Microscopy platform at Université Pierre et Marie Curie. This work has benefited from the financial support of the LabeX LaSIPS (ANR-10-LABX-0040-LaSIPS) managed by the French National Research Agency under the "Investissements d'avenir" program (n°ANR-11-IDEX-0003-02). This work was also supported by an endowment in cardiovascular cellular engineering from the AXA Research Fund. Lionel Guillou was supported by a Gaspard Monge doctoral fellowship from Ecole Polytechnique. This research has received funding from the National Institute of Health and Medical Research (INSERM), from ANR (ANR-12-BSV5-0007-01, ImmunoMeca) and Fondation pour la Recherche Médicale (FRM, FRM DEQ20140329513). MS was financed by FRM and AB was financed by la Ligue contre le Cancer and l'Association de Recherche contre le Cancer (ARC).

REFERENCES

von Andrian, U. H., and Mempel, T. R. (2003). Homing and cellular traffic in lymph nodes. Nat. Rev. Immunol. *3*, 867–878.

Bajno, L., Peng, X. R., Schreiber, A. D., Moore, H. P., Trimble, W. S., and Grinstein, S. (2000). Focal exocytosis of VAMP3-containing vesicles at sites of phagosome formation. J. Cell Biol. *149*, 697–705.

Blanchard, N., Lankar, D., Faure, F., Regnault, A., Dumont, C., Raposo, G., and Hivroz, C. (2002). TCR Activation of Human T Cells Induces the Production of Exosomes Bearing the TCR/CD3/ Complex. J. Immunol. *168*, 3235–3241.

Boesen, A. M., and Hokland, P. (1982). Stereological Analysis of the Ultrastructure in Isolated Human T and Non-T Lymphoid Cells. Cell Pathol *39*, 273–284.

Braun, V., Fraisier, V., Raposo, G., Hurbain, I., Sibarita, J.-B., Chavrier, P., Galli, T., and Niedergang, F. (2004). TI-VAMP/VAMP7 is required for optimal phagocytosis of opsonised particles in macrophages. EMBO J. *23*, 4166–4176.

Bufi, N., Saitakis, M., Dogniaux, S., Buschinger, O., Bohineust, A., Richert, A., Maurin, M., Hivroz, C., and Asnacios, A. (2015). Human primary immune cells exhibit distinct mechanical properties that are modified by inflammation. Biophys. J. *108*, 2181–2190.

Carman, C. V (2009). Mechanisms for transcellular diapedesis: probing and pathfinding by "invadosome-like protrusions". J. Cell Sci. *122*, 3025–3035.

Carman, C. V., and Martinelli, R. (2015). T lymphocyte-endothelial interactions: Emerging understanding of trafficking and antigen-specific immunity. Front. Immunol. *6*.

Carman, C. V., and Springer, T. A. (2004). A transmigratory cup in leukocyte diapedesis both through individual vascular endothelial cells and between them. J. Cell Biol. *167*, 377–388.

Cartagena-Rivera, A. X., Logue, J. S., Waterman, C. M., and Chadwick, R. S. (2016). Actomyosin Cortical Mechanical Properties in Nonadherent Cells Determined by Atomic Force Microscopy. Biophys. J. *110*, 2528–2539.

Chemin, K., Bohineust, A., Dogniaux, S., Tourret, M., Guégan, S., Miro, F., and Hivroz, C. (2012). Cytokine secretion by CD4+ T cells at the immunological synapse requires Cdc42-dependent local actin remodeling but not microtubule organizing center polarity. J. Immunol. *189*, 2159–2168.

Crotty, S. (2015). A brief history of T cell help to B cells. Nat. Rev. Immunol. *15*, 185–189.

Dimitriadis, E. K., Horkay, F., Maresca, J., Kachar, B., and Chadwick, R. S. (2002). Determination of elastic moduli of thin layers of soft material using the atomic force microscope. Biophys. J. *82*, 2798–2810.

DuPage, M., and Bluestone, J. A. (2016). Harnessing the plasticity of CD4(+) T cells to treat immune-mediated disease. Nat Rev Immunol *16*, 149–163.

Edelstein, A., Amodaj, N., Hoover, K., Vale, R., and Stuurman, N. (2010). Computer control of microscopes using manager. Curr. Protoc. Mol. Biol., 1–17.

Evans, E., Heinrich, V., Ludwig, F., and Rawicz, W. (2003). Dynamic Tension Spectroscopy and Strength of Biomembranes. Biophys. J. *85*, 2342–2350.

Evans, E., and Kukan, B. (1984). Passive material behavior of granulocytes based on large deformation and recovery after deformation tests. Blood *64*, 1028–1035.

Figard, L., Xu, H., Garcia, H., Golding, I., and Sokac, A. (2013). The plasma membrane flattens out to fuel cell-surface growth during drosophila cellularization. Dev. Cell *27*, 648–655.

Fung, Y. (2013). Biomechanics: circulation, Springer Science & Business Media.

Gauthier, N. C., Fardin, M. A., Roca-Cusachs, P., and Sheetz, M. P. (2011). Temporary increase in plasma membrane tension coordinates the activation of exocytosis and contraction during cell spreading. Proc. Natl. Acad. Sci. U. S. A. *108*, 14467–14472.

Geddes, D. M., Cargill, R. S., and LaPlaca, M. C. (2003). Mechanical stretch to neurons results in a strain rate and magnitude-dependent increase in plasma membrane permeability. J. Neurotrauma *20*, 1039–1049.

Groulx, N., Boudreault, F., Orlov, S. N., and Grygorczyk, R. (2006). Membrane reserves and hypotonic cell swelling. J. Membr. Biol. *214*, 43–56.

Guillou, L., Babataheri, A., Puech, P.-H., Barakat, A. I., and Husson, J. (2016). Dynamic monitoring of cell mechanical properties using profile microindentation. Sci. Rep. *6*, 21529.

Hackam, D. J., Rotstein, O. D., Sjolin, C., Schreiber, a D., Trimble, W. S., and Grinstein, S. (1998). v-SNARE-dependent secretion is required for phagocytosis. Proc. Natl. Acad. Sci. U. S. A. *95*, 11691–11696.

Hategan, A., Law, R., Kahn, S., and Discher, D. E. (2003). Adhesively-tensed cell membranes: lysis kinetics and atomic force microscopy probing. Biophys. J. *85*, 2746–2759.

Herant, M., Heinrich, V., and Dembo, M. (2005). Mechanics of neutrophil phagocytosis: behavior of the cortical tension. J. Cell Sci. *118*, 1789–1797.

Hochmuth, R. M. (2000). Micropipette aspiration of living cells. J. Biomech. *33*, 15–22.

Johnson, K. L. (1985). Contact Mechanics. J. Am. Chem. Soc. *37*, 1–17.

Krause, M., te Riet, J., and Wolf, K. (2013). Probing the compressibility of tumor cell nuclei by combined atomic force–confocal microscopy. Phys. Biol. *10*, 065002.

Lam, J., Herant, M., Dembo, M., and Heinrich, V. (2009). Baseline Mechanical Characterization of J774 Macrophages. Biophys. J. *96*, 248–254.

Lomakina, E. B., Spillmann, C. M., King, M. R., and Waugh, R. E. (2004). Rheological analysis and measurement of neutrophil indentation. Biophys. J. *87*, 4246–4258.

Majstoravich, S., Zhang, J., Nicholson-Dykstra, S., Linder, S., Friedrich, W., Siminovitch, K. A., and Higgs, H. N. (2004). Lymphocyte microvilli are dynamic, actin-dependent structures that do not require Wiskott-Aldrich syndrome protein (WASp) for their morphology. Blood *104*, 1396–1403.

Niedergang, F., Colucci-Guyon, E., Dubois, T., Raposo, G., and Chavrier, P. (2003). ADP ribosylation factor 6 is activated and controls membrane delivery during phagocytosis in macrophages. J. Cell Biol. *161*, 1143–1150.

Petrie, R. J., Koo, H., and Yamada, K. M. (2014). Generation of compartmentalized pressure by a nuclear piston governs cell motility in a 3D matrix. Science (80-.). *345*, 1062–1065.

Pettus, E. H., Christman, C. W., Giebel, M. L., and Povlishock, J. T. (1994). Traumatically induced altered membrane permeability: its relationship to traumatically induced reactive axonal change. J. Neurotrauma *11*, 507–522.

Pettus, E. H., and Povlishock, J. T. (1996). Characterization of a distinct set of intra-axonal ultrastructural changes associated with traumatically induced alteration in axolemmal permeability. Brain Res. *722*, 1–11.

Ross, P. E., Garber, S. S., and Cahalan, M. D. (1994). Membrane chloride conductance and capacitance in Jurkat T lymphocytes during osmotic swelling. Biophys. J. *66*, 169–178.

Schmid-Schönbein, G. W., Shih, Y. Y., and Chien, S. (1980). Morphometry of human leukocytes. Blood *56*, 866–875.

Shulman, Z. *et al.* (2011). Transendothelial migration of lymphocytes mediated by intraendothelial vesicle stores rather than by extracellular chemokine depots. Nat Immunol *13*, 67–76.

Spinler, K. R., Shin, J. W., Lambert, M. P., and Discher, D. E. (2015). Myosin-II repression favors pre/proplatelets but shear activation generates platelets and fails in macrothrombocytopenia. Blood *125*, 525–533.

Springer, T. A. (1994). Traffic signals for lymphocyte recirculation and leukocyte emigration: The multistep paradigm. Cell *76*, 301–314.

Tan, S. C. W., Yang, T., Gong, Y., and Liao, K. (2011). Rupture of plasma membrane under tension. J. Biomech. *44*, 1361–1366.

Valignat, M. P., Theodoly, O., Gucciardi, A., Hogg, N., and Lellouch, A. C. (2013). T lymphocytes orient against the direction of fluid flow during LFA-1-mediated migration. Biophys. J. *104*, 322–331.

Wakatsuki, T., Schwab, B., Thompson, N. C., and Elson, E. L. (2001). Effects of cytochalasin D and latrunculin B on mechanical properties of cells. J. Cell Sci. *114*, 1025–1036.

FIGURE CAPTIONS

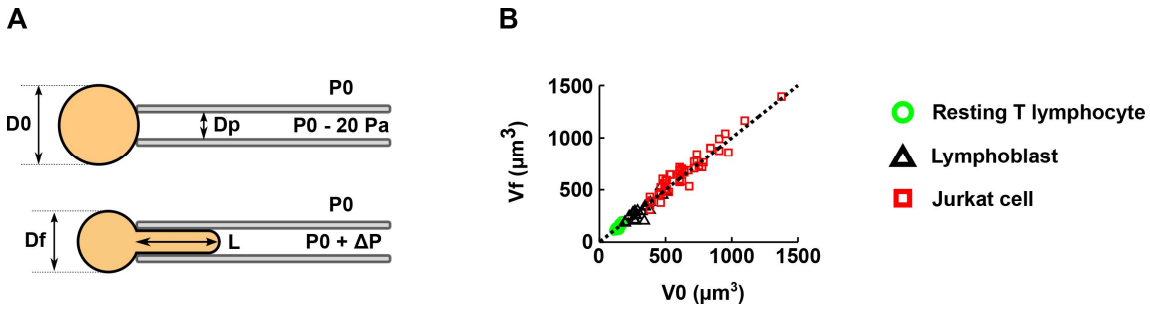

FIGURE 1: T lymphocyte volume is conserved during micropipette aspiration. (A) Diagram of a micropipette aspiration experiment. We impose an aspiration pressure P0+ΔP (ΔP assumes only negative values) and measure the initial cell diameter D0, the final cell diameter Df, the micropipette diameter Dp and the final entry length L. (B) Plot of the final cell volume Vf (see Supplementary Figure S1 for details on volume measurement), as a function of the initial cell volume V0. Data points fall on the dotted line of slope one (Vf = V0), showing that cell volume is conserved.

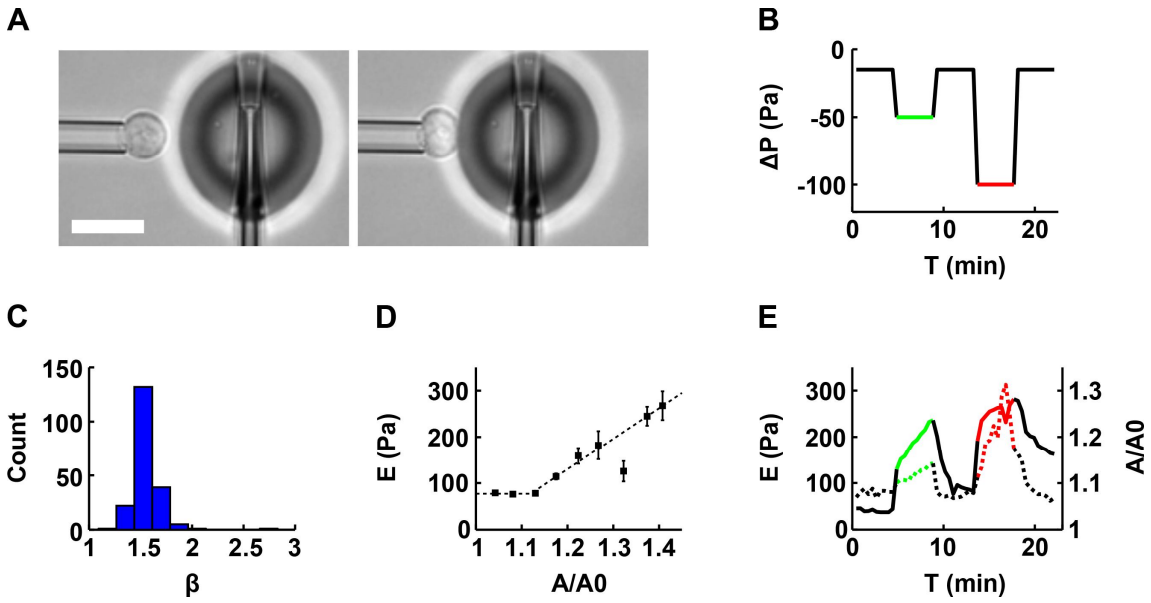

FIGURE 2: Resting T lymphocyte's apparent stiffness increases with apparent membrane surface area. (A) Example of a resting T lymphocyte being aspirated into a micropipette while its apparent stiffness is measured using profile microindentation. Scale bar is 10 µm. (B) Plot of the aspiration pressure ΔP used to hold the resting T lymphocytes during profile microindentation as a function of time. Each resting T lymphocyte is indented approximately 50 times, once every 30 seconds. In black, aspiration pressure is -15 Pa, green is -50 Pa and red is -100 Pa. (C) Histogram of the indentation scaling exponent β found during the profile microindentations. We fit the force-indentation curve using the relation $F = \alpha\, \delta^{\beta}$, with F the force, δ the indentation, and α and β two fitting parameters. (D) Plot of the apparent stiffness E as a function of the normalized apparent membrane surface area A/A0, where A0 is the initial membrane surface area and A the membrane surface area at the time where the apparent stiffness E is measured. Bars represent the standard deviation. We have N = 5 cells and n = 201 microindentations. The number of cells decreases for large values of A/A0. The 3 last points to the right correspond to only 5, 7 and 2 microindentations respectively, compared to more than 30 on average for the 6 points to the left. Dotted line represents the best fit using the phenomenological relation $E = E0$ for $A/A0<(1+\varepsilon)$ and $E = E0 + k\,(A/A0-(1+\varepsilon))$ for $A/A0>(1+\varepsilon)$. (E) Plot of the apparent stiffness E (left axis, dotted line) and the normalized apparent membrane surface area A/A0 (right axis, continuous line) averaged over n = 5 cells, as a function of time.

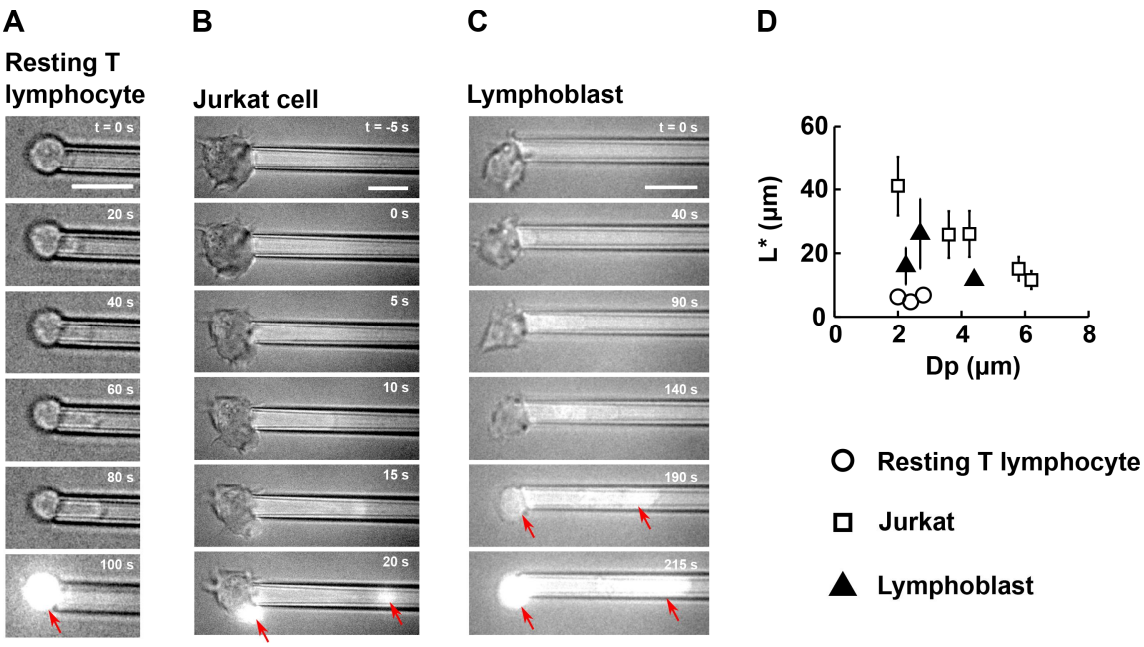

FIGURE 3: T lymphocyte membrane ruptures at a well-defined entry length L* during micropipette aspiration. (A-C) Example of membrane rupture triggered using micropipette aspiration for (A) a resting T lymphocyte, (B) a Jurkat cell and (C) a lymphoblast. Scale bar is 10 µm. The time is indicated in the top right hand corner, with t = 0 s chosen as the time at which the aspiration pressure goes from - 20 Pa to ΔP. A background of brightfield light is kept to visualize the cell throughout the experiment. Upon membrane rupture, propidium iodide enters the cell and binds to DNA, emitting a bright fluorescent signal (red arrows). (D) Plot of the entry length at rupture L* versus the micropipette diameter Dp for three cell types: resting T lymphocytes (n = 14 cells), Jurkat cells (n = 27 cells) and lymphoblasts (n = 14 cells). Bars represent the standard deviation.

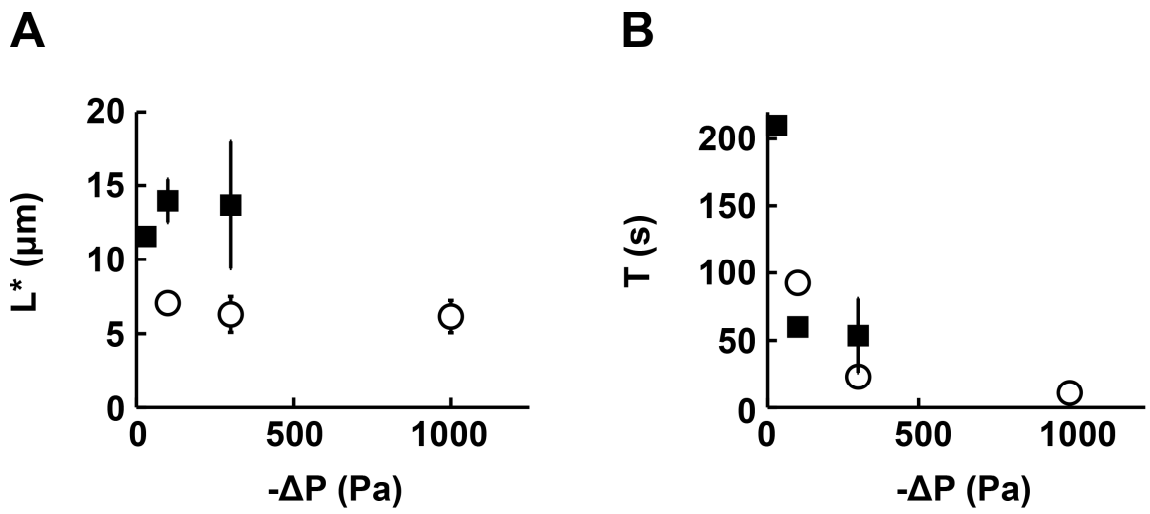

FIGURE 4: Effect of the aspiration pressure on T lymphocyte membrane rupture. (A) Plot of the entry length at rupture L* as a function of the absolute value of the aspiration pressure ΔP for resting T lymphocytes (white circles) and Jurkat cells (black squares). (B) Plot of the duration of micropipette aspiration T to rupture as a function of the absolute value of aspiration pressure ΔP for resting T lymphocytes (white circles) and Jurkat cells (black squares). Bars indicate standard deviation. For resting T lymphocytes, micropipette diameters between 2.0 and 2.8 µm were included (n = 14 ruptured cells). For Jurkat cells, micropipette diameters between 5.8 and 6.2 µm were included (n = 10 ruptured cells).

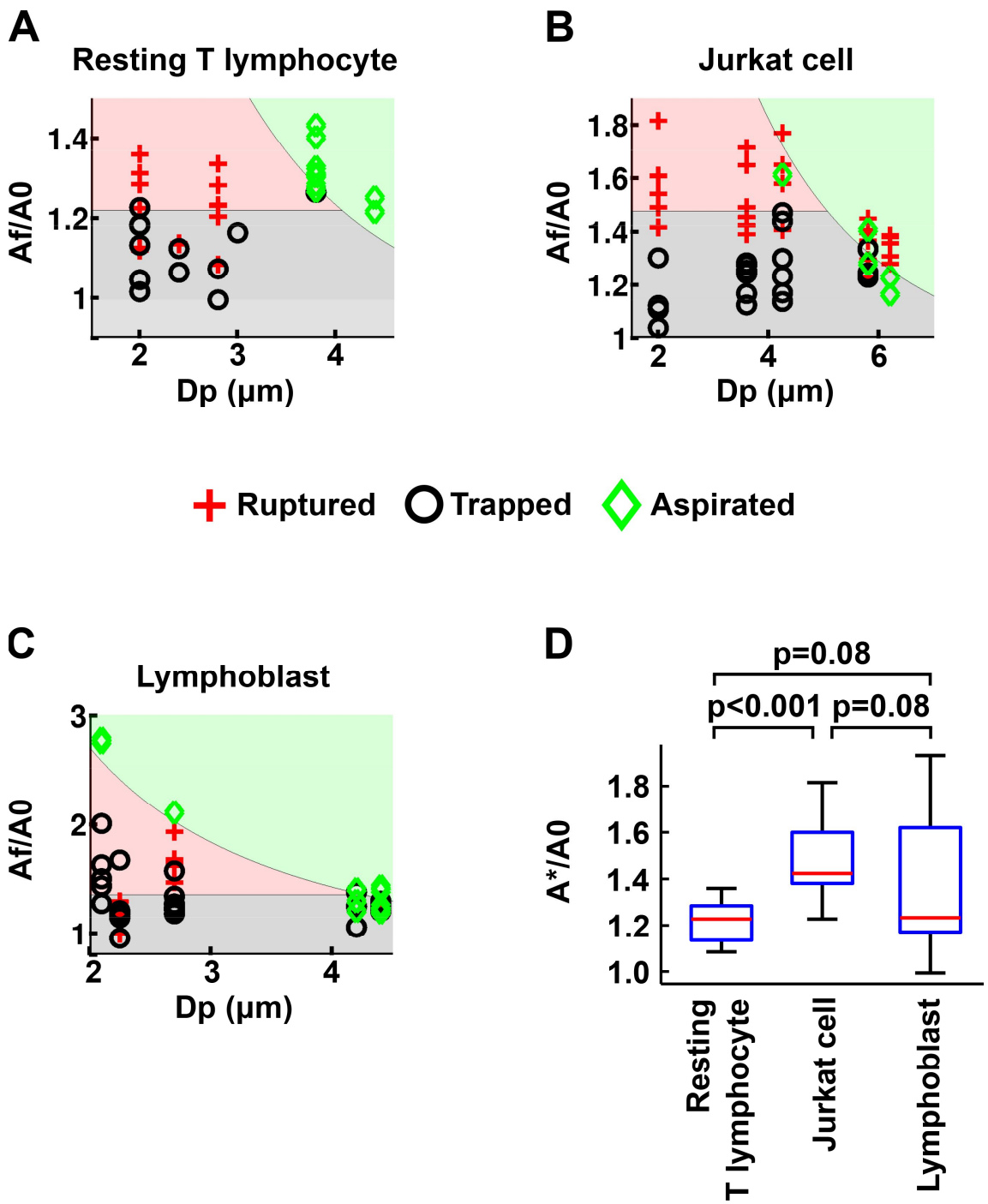

FIGURE 5: T lymphocyte membrane rupture occurs at a critical increase in apparent membrane surface area A*/A0. (A-C) "Phase diagram" of cell state after micropipette aspiration, depending on the micropipette diameter Dp and the membrane expansion, defined as the final apparent membrane surface area Af divided by the initial apparent membrane surface area A0. The phase diagrams are given for various cell types and conditions: (A) resting T lymphocytes, (B) Jurkat cells and (C) lymphoblasts. As shown in the legend, a red cross indicates a cell whose membrane ruptured, a black circle a cell that stayed trapped after 5 minutes of aspiration, and a

green diamond a cell that was entirely aspirated inside the micropipette. The red filling indicates that in this zone, cell membranes are expected to rupture. The grey filling indicates that in this zone, a cell is expected to stay trapped inside the micropipette without rupturing or being entirely aspirated. The cutoff on the vertical axis between the red and the grey zone is chosen as the mean increase in apparent membrane surface area. The green filling indicates that in this zone, cells are expected to be entirely aspirated based on geometrical considerations and volume conservation (Supplementary Movie 6). (D) Boxplot of the normalized apparent membrane surface area at rupture A*/A0 for the cell types and conditions reported in (A-C).

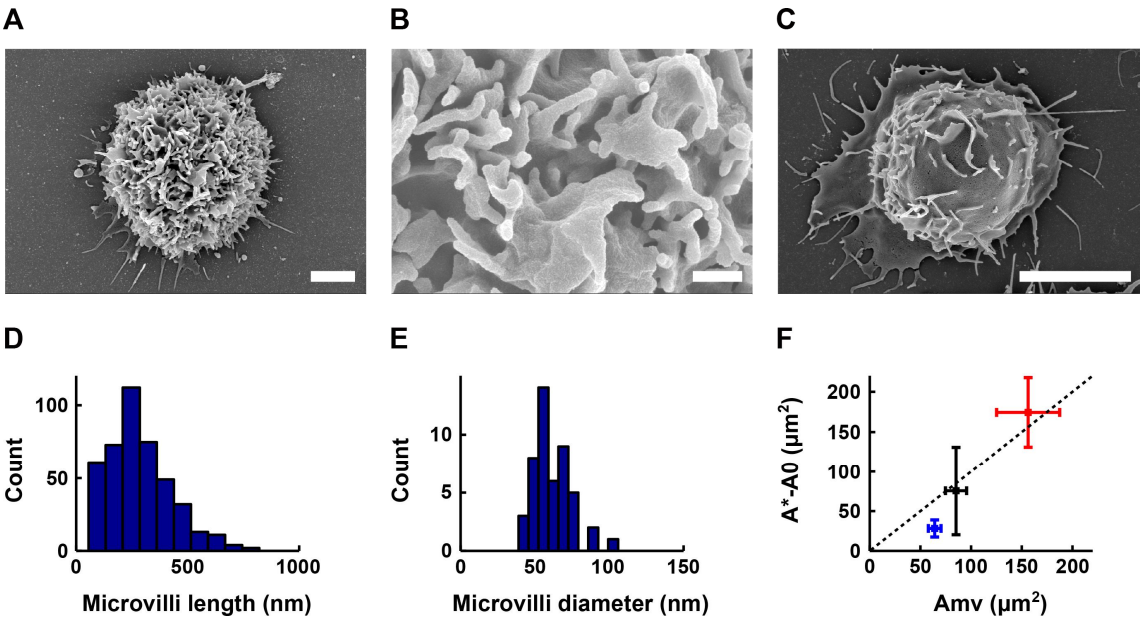

FIGURE 6: Maximum membrane surface area increase during micropipette aspiration is of the same order of magnitude as the excess membrane contained in microvilli and membrane folds. (A-C) Scanning electron microscopy images of a lymphoblast (A, B) and a Jurkat cell (C). Scale bars are 2 μm (A), 400 nm (B) and 5 μm (C). (D) Histogram of lymphoblasts' microvilli lengths (n = 432 measurements, N = 10 cells). We find the length is 284 ± 140 nm (mean ± SD). (E) Histogram of lymphoblasts' microvilli diameters (n = 48 measurements, N = 1 cell, as we observed that the diameter was well conserved across cells). We find the diameter is 62 ± 13 nm (mean ± SD). (F) Plot of the maximum increase in apparent membrane surface area during micropipette aspiration experiments (defined as the apparent membrane surface area at rupture A* minus the initial apparent membrane surface area A0) as a function of the estimated excess membrane contained in microvilli and membrane folds, Amv, for resting T lymphocytes (blue), Jurkat cells (red) and lymphoblasts (black). Squares represent the mean, bars represent the standard deviation. Dotted line represents the A*-A0 = Amv (slope equal to 1) line.

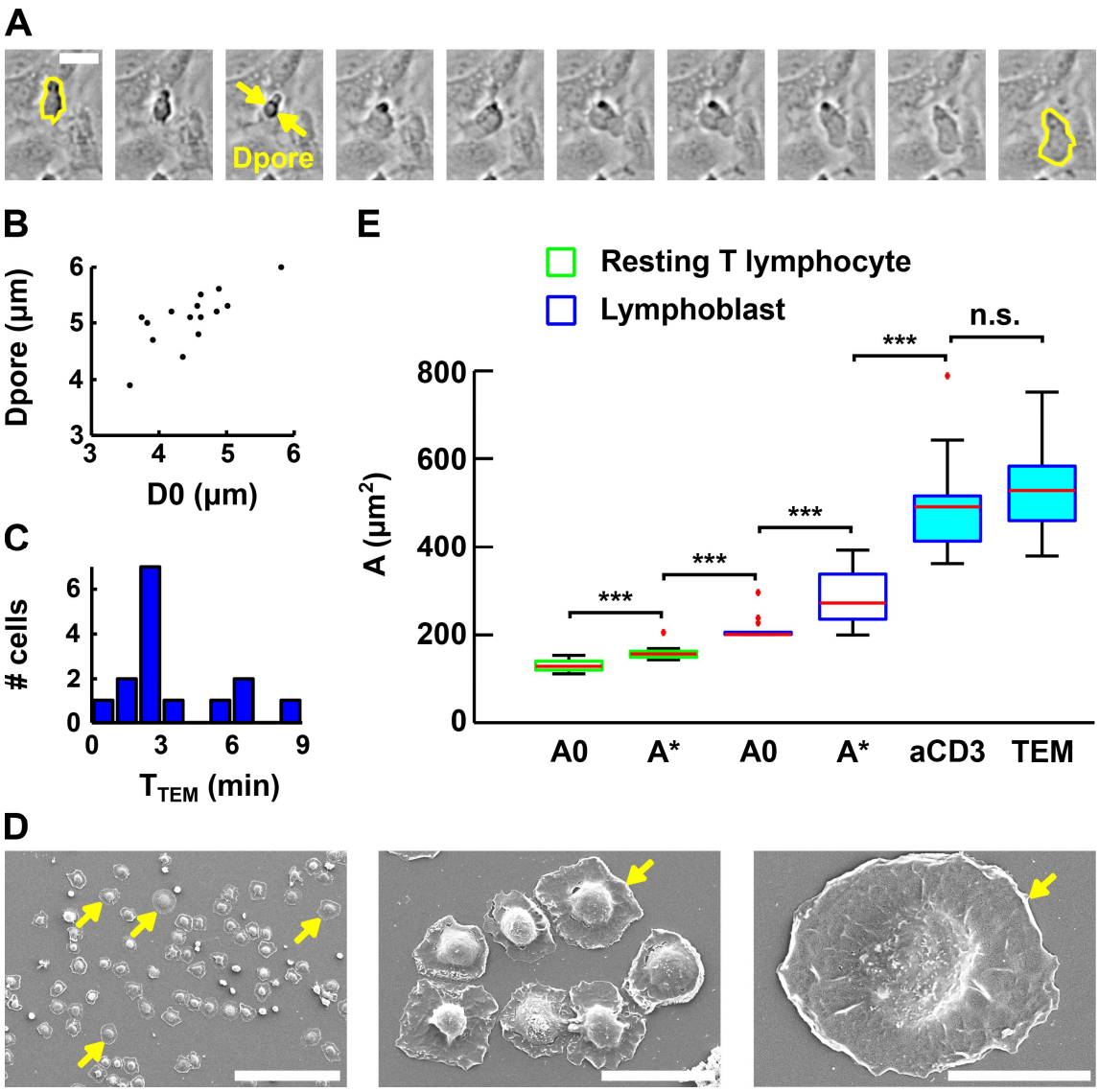

FIGURE 7: Evolution of lymphoblasts' membrane surface area during transendothelial migration and cell spreading. (A) Time lapse of a lymphoblast transmigrating between human aortic endothelial cells. Scale bar is 20 µm. Images are taken every 15 seconds. The projected surface area Sproj is represented in yellow before (left-most image) and after (right-most image) transendothelial migration. The pore diameter Dpore is estimated by taking the image in which the lymphoblast width is identical both above and below the pore (yellow arrows). (B) Pore diameter Dpore during transendothelial migration as a function of the lymphoblast's projected diameter before transendothelial migration (computed using $D0 = Sproj / 2\pi$, where Sproj is the projected surface area and D0 an equivalent diameter for a sphere whose projected area is Sproj). (C) Histogram of the duration of transmigration. The mean duration is 3 ± 2 min (mean ± SD). (D) Scanning electron microscopy images of lymphoblasts spreading on a substrate coated with anti-CD3+anti-CD28 activating antibodies. Scale bars from left to right are 100 µm, 20 µm and 10 µm. Yellow arrows

indicate spread cells. (E) Boxplots of the apparent membrane surface area of T lymphocytes under both passive (white-filled box) and active (blue-filled box) deformations. The bottom and top of the box indicate the 25^{th} and the 75^{th} percentile, respectively. Red '+' symbols indicate outliers. From left to right, we have: resting T lymphocytes initially (column 1, A0, n = 14) and at rupture (column 2, A*, n = 14) aspirated using a micropipette, lymphoblasts at rest (column 3, A0, n = 14) and at rupture (column 4, A*, n = 14) aspirated using a micropipette, lymphoblasts spread on anti-CD3+anti-CD28 mAbs (column 5, aCD3, n = 17), and lymphoblasts after transendothelial migration (column 6, TEM, n = 15). *** indicates $p<0.001$. n.s. indicates $p>0.05$.

Supplemental Materials

Molecular Biology of the Cell

Guillou et al.

SUPPLEMENTARY MATERIAL

SUPPLEMENTARY FIGURE S1: Equations for computing the area and volume of a cell aspirated into a micropipette.

We assume that micropipette aspiration of a cell constitutes an axisymmetric system around the axis of the micropipette.

The initial cell volume before aspiration is:

$$V0 = \frac{4}{3}\pi(\frac{D0}{2})^3$$

During aspiration, the height and volume of the small dome that needs to be subtracted are:

$$hdome = \frac{Df}{2} - ((\frac{Df}{2})^2 - (\frac{Dp}{2})^2)^{1/2}$$

$$Vdome = \frac{hdome}{6}\pi(3(\frac{Dp}{2})^2 + hdome^2)$$

The final volume during aspiration is:

$$Vf = \frac{4}{3}\pi(\frac{Df}{2})^3 - Vdome + \pi(\frac{Dp}{2})^2 L + \frac{2}{3}\pi(\frac{Dp}{2})^3$$

The initial cell area before aspiration is:

$$A0 = \pi(D0)^2$$

During aspiration, the area of the small dome that needs to be subtracted is:

$$Adome = 2\pi(\frac{Df}{2})hdome$$

The final cell area during aspiration is:

$$Af = \pi(Df)^2 - Adome + \pi(Dp)L + 2\pi(\frac{Dp}{2})^2$$

SUPPLEMENTARY FIGURE S2: Fluorescent staining of T lymphocytes used to estimate cell volume. F-actin is in red and nucleus is in blue. Scale bar is 5 µm. We find V0 = 274 ± 75 µm^3 (n = 298), 473 ± 136 µm^3 (n = 143) and 797 ± 250 µm^3 (n = 68) (mean ± SD) for resting T lymphocytes, lymphoblasts and Jurkat cells respectively. This is slightly higher than the apparent volume we estimated using optical microscopy of cells in suspension, but still in good agreement.

SUPPLEMENTARY FIGURE S3: Compressive force F exerted on a cell during microindentation, as a function of the indentation δ. The raw data, in grey, are acquired at a frequency of ~350 Hz. In blue we plot a moving average of the raw data over 50 points. In red, we overlay the best fit found using the Hertz model.

SUPPLEMENTARY FIGURE S4: The relationship between the apparent stiffness and the apparent membrane surface area is reversible. (A) Plot of the apparent stiffness E as a function of the normalized apparent membrane surface area A/A0, where A0 is the initial membrane surface area and A the membrane surface area at the time where the apparent stiffness E is measured. We have N = 5 cells (resting T lymphocytes) and n = 201 microindentations. Black dots represent measurements for which ΔP = - 15 Pa, green dots those for which ΔP = - 50 Pa and red dots those for which ΔP = - 100 Pa. The dotted line represents the best fit using the phenomenological relation $E = E0$ for $A/A0<(1+\varepsilon)$ and $E = E0 + k(A/A0-(1+\varepsilon))$ for $A/A0>(1+\varepsilon)$.

SUPPLEMENTARY FIGURE S5: Myosin-II activity softens resting T lymphocytes. (A) Normalized apparent membrane surface area A/A0, where A0 is the initial membrane surface area and A the membrane surface area, as a function of time T. An aspiration pressure of ΔP = -300 Pa is applied for T between 220 and 440 seconds. Before and after that, we have ΔP = -30 Pa. Bars represent the standard deviation. In black, control cells (N = 13 cells, n = 429 microindentations) and in blue, blebbistatin treated cells (N = 8 cells, n = 212 microindentations). Membrane surface area was measured at every indentation

cycle. (B) Apparent stiffness E, as measured by microindentation, as a function of time T. These data show the apparent stiffness of the cells in panel A. Therefore, the same profile of aspiration pressure over time applies here. Also, the same color code and conventions apply as in panel A.

SUPPLEMENTARY FIGURE S6: Effect of aspiration pressure on Jurkat cell membrane rupture. (A) Plot of the membrane expansion at rupture A*/A0, as a function of the absolute value of the aspiration pressure ΔP for Jurkat cells (n = 22 ruptured cells). (B) Plot of the duration T of micropipette aspiration before rupture, as a function of the absolute value of the aspiration pressure ΔP for Jurkat cells (n = 22 ruptured cells). The two aspiration pressures with the most ruptured cells (ΔP = -300 and -1000 Pa), which account for over 80% of the total number of Jurkat cell ruptures, were selected for this plot.

SUPPLEMENTARY TABLES

	Membrane slack ε	Expansion modulus k	Method of measurement for k
Resting T lymphocytes	12 ± 2%	660 ± 80 Pa	Profile microindentation
Neutrophils	6%	0.16 mN/m for A/A0 < 1.25 2.14 mN/m for A/A0 > 1.30	Micropipette aspiration at equilibrium

SUPPLEMENTARY TABLE T1: Fitting parameters in the following phenomenological law linking the effective stiffness E and apparent membrane surface increase A/A0:

$$\begin{cases} E = E0 \text{ for } A/A0 < (1+\varepsilon) \\ E = E0 + k\,(A/A0 - (1+\varepsilon)) \text{ for } A/A0 > (1+\varepsilon) \end{cases}$$

The values for resting T lymphocytes come from our own measurements and are given as mean ± standard error of the mean. The comparative values come from

a previous study by Herant *et al.* which looked at the cell tension and the membrane expansion of neutrophils at equilibrium (Herant *et al.*, 2005).

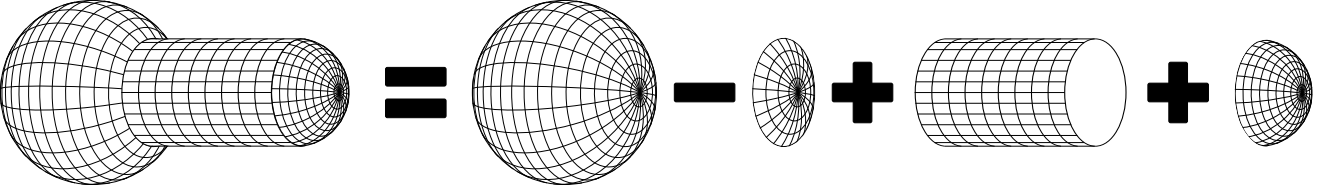

Resting T lymphocyte

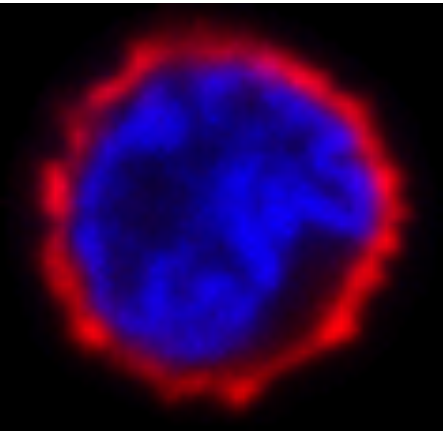

Lymphoblast

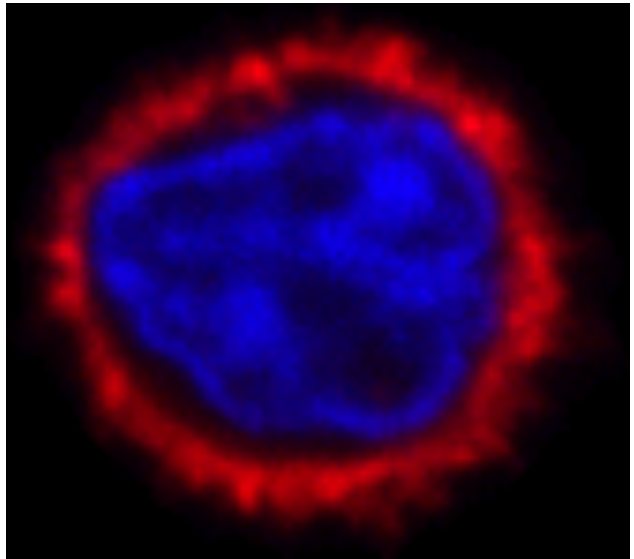

Jurkat cell

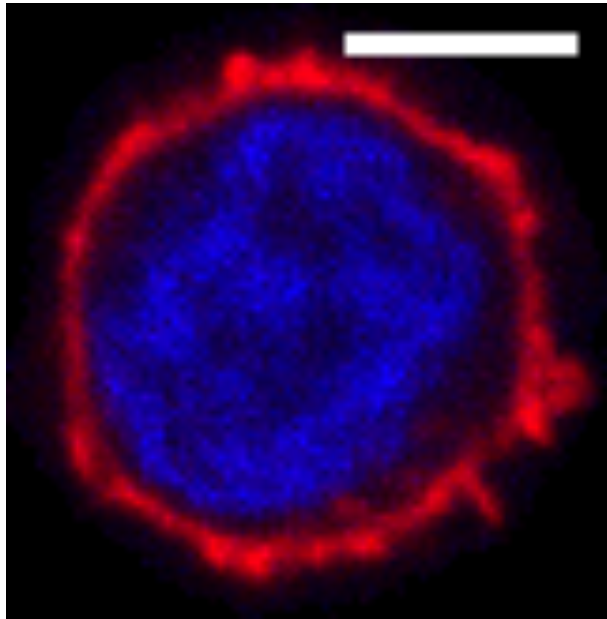

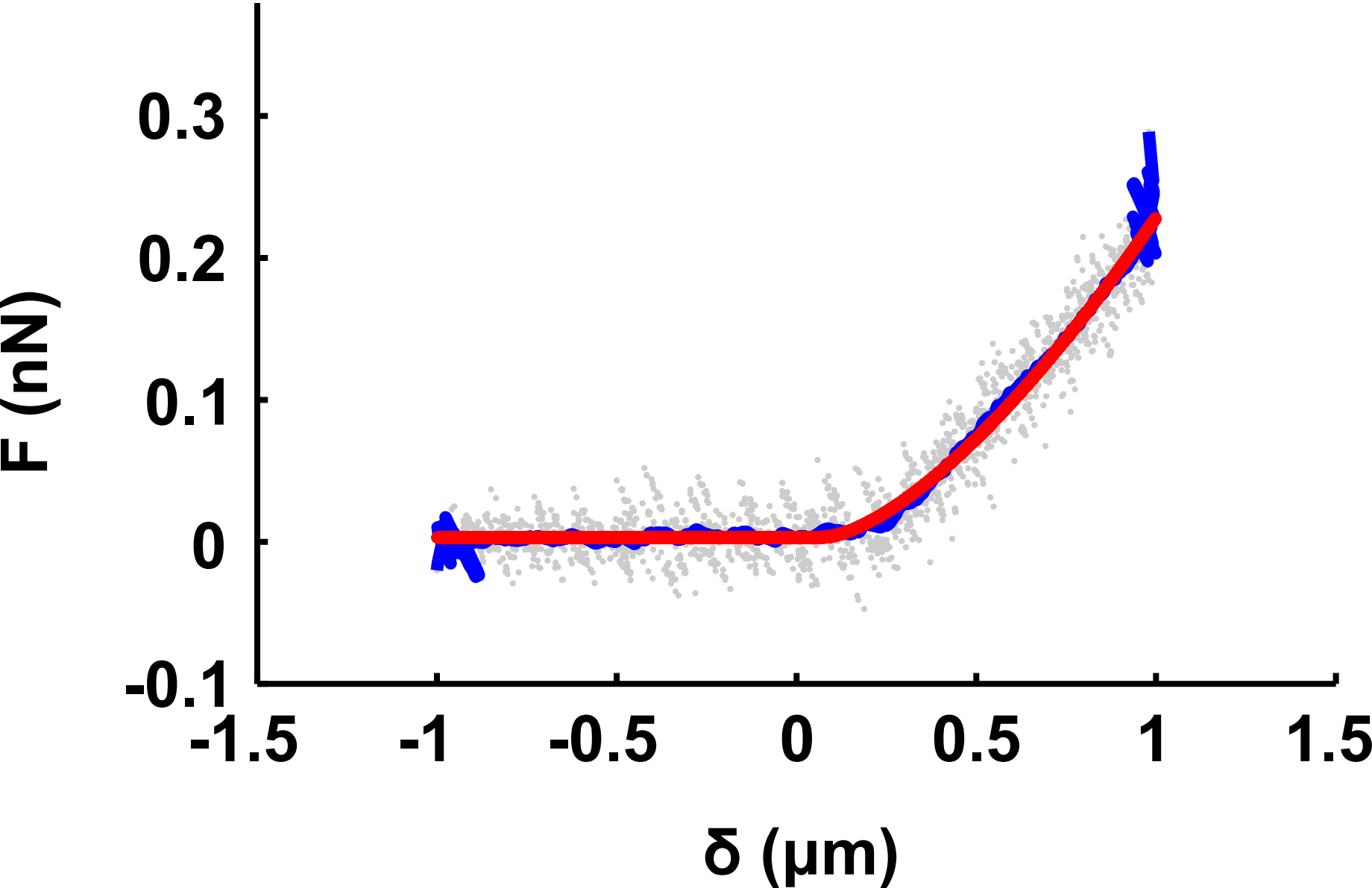
0.3
0.2
0.1
0
-0.1
F (nN)
-1.5
-1
-0.5
0
0.5
1
1.5
δ (μm)

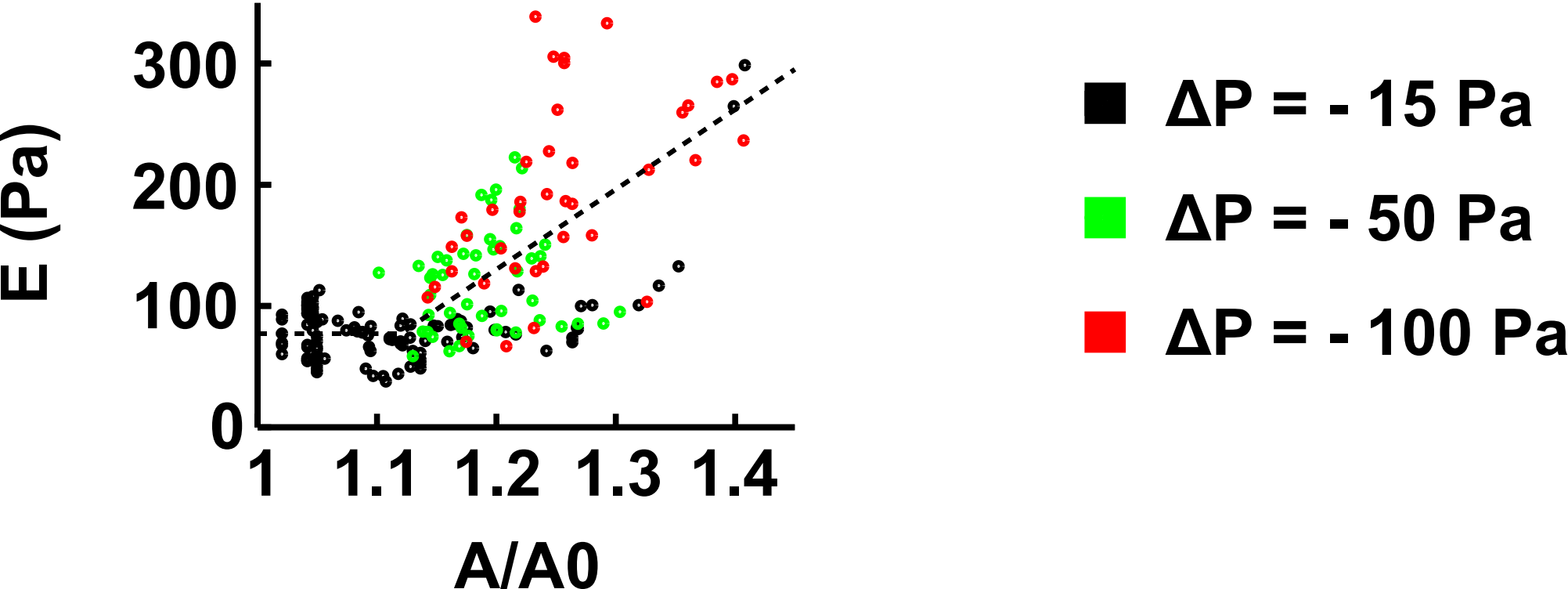
E (Pa)
300
200
100
0
1
1.1
1.2
1.3
1.4
A/A0
ΔP = - 15 Pa
ΔP = - 50 Pa
ΔP = - 100 Pa

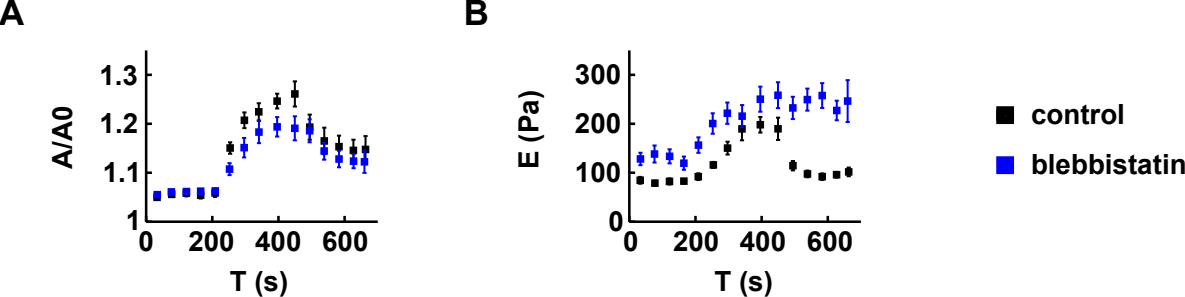
A
A/A0
1.3
1.2
1.1
1
0
200
400
600
T (s)
B
E (Pa)
300
200
100
0
0
200
400
600
T (s)
control
blebbistatin

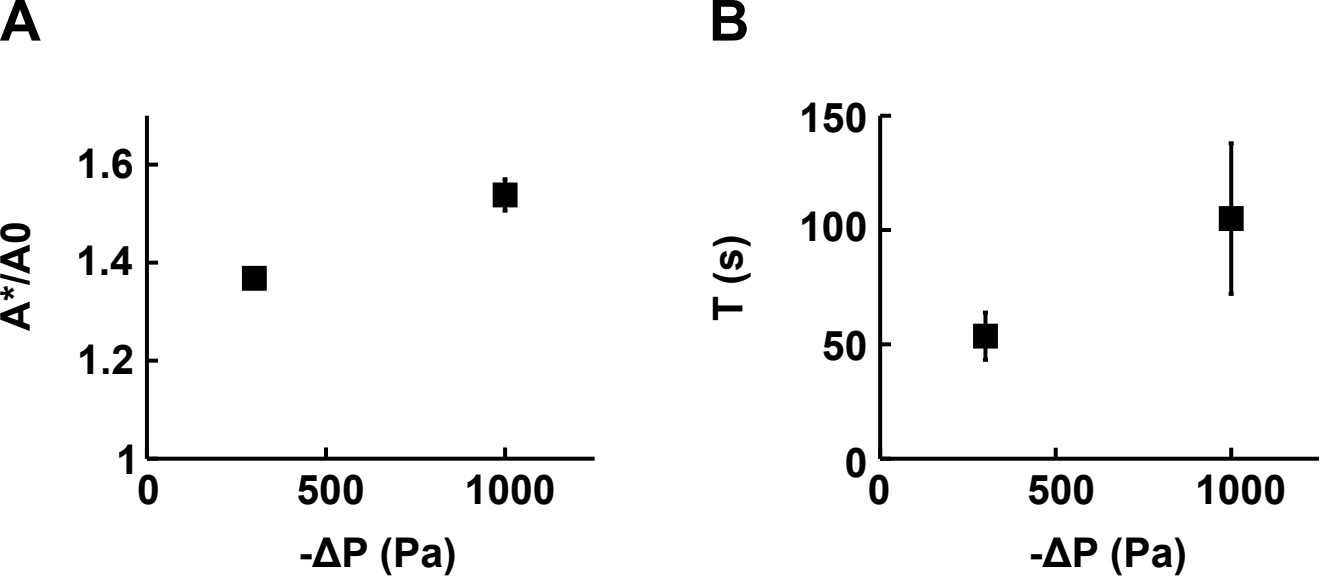
A
A*/A0
1.6
1.4
1.2
1
0
500
1000
-ΔP (Pa)
B
T (s)
150
100
50
0
0
500
1000
-ΔP (Pa)